

# Quenched chiral logarithms in lattice QCD with exact chiral symmetry

Ting-Wai Chiu and Tung-Han Hsieh

Department of Physics, National Taiwan University  
Taipei, Taiwan 106, Taiwan.  
*E-mail* : *twchiu@phys.ntu.edu.tw*

## Abstract

We examine quenched chiral logarithms in lattice QCD with overlap Dirac quark. For 100 gauge configurations generated with the Wilson gauge action at  $\beta = 5.8$  on the  $8^3 \times 24$  lattice, we compute quenched quark propagators for 12 bare quark masses. The pion decay constant is extracted from the pion propagator, and from which the lattice spacing is determined to be 0.147 fm. The presence of quenched chiral logarithm in the pion mass is confirmed, and its coefficient is determined to be  $\delta = 0.203 \pm 0.014$ , in agreement with the theoretical estimate in quenched chiral perturbation theory. Further, we obtain the topological susceptibility of these 100 gauge configurations by measuring the index of the overlap Dirac operator. Using a formula due to exact chiral symmetry, we obtain the  $\eta'$  mass in quenched chiral perturbation theory,  $m_{\eta'} = (901 \pm 64)$  MeV, and an estimate of  $\delta = 0.197 \pm 0.027$ , which is in good agreement with that determined from the pion mass.

PACS numbers: 11.15.Ha, 11.30.Rd, 12.38.Gc

Keywords : Chiral Perturbation Theory, Chiral Symmetry, Lattice Gauge Theory, Lattice QCD, Overlap Dirac Quark.

# 1 Introduction

In quenched chiral perturbation theory [1, 2], it has been asserted that some quantities in QCD possess logarithmic dependence on the bare quark masses as the latter approach zero, similar to the unquenched case. In particular, for the pseudoscalar meson mass and the condensate, there are extra chiral logarithms due to the  $\eta'$  loop void of topological screening in the quenched approximation. Explicitly, the pion mass to one-loop order can be written as

$$m_\pi^2 = Cm_q\{1 - \delta[\ln(Cm_q/\Lambda_\chi^2) + 1]\} + Bm_q^2, \quad (1)$$

where  $m_q$  denotes the bare ( $u$  and  $d$ ) quark mass,  $\Lambda_\chi$  the chiral cutoff which can be taken to be  $2\sqrt{2}\pi f_\pi$  ( $f_\pi \simeq 132$  MeV),  $C$  and  $B$  are parameters, and  $\delta$  the coefficient of the quenched chiral logarithm.

Theoretically,  $\delta$  can be estimated to be [1]

$$\delta = \frac{m_{\eta'}^2}{8\pi^2 f_\pi^2 N_f}, \quad (2)$$

where  $m_{\eta'}$  denotes the  $\eta'$  mass in quenched chiral perturbation theory,  $f_\pi$  the pion decay constant, and  $N_f$  the number of light quark flavors. For  $m_{\eta'} = 900$  MeV,  $f_\pi = 132$  MeV, and  $N_f = 3$ , (2) gives  $\delta \simeq 0.2$ . Evidently, if one can extract  $\delta$  from the data of  $m_\pi^2$  in lattice QCD, then  $m_{\eta'}$  in quenched chiral perturbation theory can be determined by (2).

Presumably, the chiral logarithm in (1) can be observed unambiguously in quenched lattice QCD. However, it is rather difficult to disentangle a logarithm from a power series. So far, there is no compiling evidence to single out (1) among many functional forms which seemingly can fit the data of  $m_\pi^2$  very well (e.g.,  $m_\pi^2 = A + Cm_q + Bm_q^2$ ).

For lattice QCD with Wilson-Dirac quark, the chiral symmetry is explicitly broken and the quark mass is additively renormalized, thus one does not expect that quenched chiral logarithm can be identified unambiguously at finite lattice spacing. In fact, if one tries to fit (1) to the data of  $m_\pi^2$  with Wilson-Dirac quark, one would obtain the coefficient of quenched chiral logarithm,  $\delta \simeq 0.06 - 0.12$  [3, 4], quite smaller than its theoretical expectation 0.2. For lattice QCD with staggered quark, the coefficient of chiral logarithm also turns out to be rather small,  $\delta \simeq 0.06$  [5], similar to the case of Wilson-Dirac quark. These discrepancies indicate that quenched chiral logarithm may not be properly reproduced in lattice QCD with these two lattice fermion schemes, at finite lattice spacing.

With the realization of exact chiral symmetry on the lattice, one expects that quenched chiral logarithm can be reproduced in lattice QCD with overlap Dirac quarks [6, 7]. In a recent study [8], the coefficient of quenched chiral logarithm  $\delta$  is estimated to be in the range 0.15 – 0.4 for the chiral cutoff

$\Lambda_\chi$  in the range 0.6 – 1.0 GeV, by fitting (1) to their data of  $m_\pi^2$ . At  $\Lambda_\chi a = 2\sqrt{2}\pi f_\pi a = 1.17$  GeV, their data seems to give  $\delta \simeq 0.41(9)$ , which is too large comparing with the theoretical estimate,  $\delta \sim 0.18 - 0.20$ . Thus, it is not clear whether quenched chiral logarithm has been unambiguously identified.

Besides from the data of  $m_\pi^2$ , one can also obtain  $\delta$  (2) by extracting  $m_{\eta'}$  from the propagator of the disconnected hairpin diagram. However, to compute the propagator of hairpin is very tedious. Fortunately, due to the chiral symmetry of  $D_c$  (6) in the quark propagator  $(D_c + m_q)^{-1}$ , only the zero modes of  $D_c$  can contribute to the hairpin diagram, regardless of the bare quark mass  $m_q$ . Thus one can derive an exact relation (49) between the  $\eta'$  mass in quenched chiral perturbation theory and the index susceptibility of any Ginsparg-Wilson lattice Dirac operator, without computing the hairpin diagram explicitly. Explicitly, it reads as

$$m_{\eta'}^2 = \frac{4N_f \langle (n_+ - n_-)^2 \rangle}{f_\pi^2 V} \quad (3)$$

where  $N_f$  denotes the number of light quark flavors,  $V$  the space-time volume, and  $\langle (n_+ - n_-)^2 \rangle / V$  the index susceptibility of any Ginsparg-Wilson lattice Dirac operator in the quenched approximation. Then (2) and (3) together gives

$$\delta = \frac{1}{2\pi^2 (f_\pi a)^4} \frac{\langle (n_+ - n_-)^2 \rangle}{N_s} \quad (4)$$

where  $N_s$  is the total number of sites of the lattice. A salient feature of (4) is that  $\delta$  can be determined at finite lattice spacing  $a$ , by measuring the index (susceptibility) of the overlap Dirac operator, and with  $f_\pi a$  extracted from the pion propagator. Further, we suspect that the value of  $\delta$  (4) is scale invariant at least for a range of lattice spacings including the continuum limit  $a \rightarrow 0$ .

Now it is clear that, in order to confirm the presence of quenched chiral logarithm in lattice QCD, one needs to check whether the coefficient  $\delta$  determined from the data of  $m_\pi^2$  agrees with that (4) obtained from the index susceptibility. Further, they should be close to the theoretical expectation  $\delta \simeq 0.2$ . This is a requirement for the consistency of the theory, since the quenched chiral logarithm in  $m_\pi^2$  (1) is due to the  $\eta'$  loop coupling to the pion propagator through the mass term (in the chiral lagrangian), thus  $\delta$  ( $m_{\eta'}$ ) must be the same in both cases. Otherwise, a consistent picture of the theory has not been established, and one may infer that something must have gone wrong, either in the formulation or in the implementation of the theory. We regard this consistency requirement as a basic criterion for lattice QCD (with any fermion scheme) to realize QCD chiral dynamics in continuum.

In this paper, we examine whether lattice QCD with overlap Dirac quark can satisfy this basic criterion.

## 2 Pion mass and decay constant

In this section, we set up our notations for computing quenched quark propagator as well as meson propagators in lattice QCD with exact chiral symmetry. Then we describe the practical implementation for overlap Dirac quark in our computations. Finally, we present our results of  $m_\pi^2 a^2$  and  $f_\pi a$  for 12 bare quark masses, and determine the coefficient of quenched chiral logarithm,  $\delta = 0.203 \pm 0.014$ .

### 2.1 Some general formulas

First, we recall some general formulas in lattice QCD with exact chiral symmetry. For any massless lattice Dirac operator  $D$  satisfying the Ginsparg-Wilson relation [9]

$$D\gamma_5 + \gamma_5 D = 2raD\gamma_5 D , \quad (5)$$

it can be written in terms of a chirally symmetric Dirac operator  $D_c$  [10],

$$D = D_c(1 + raD_c)^{-1} . \quad (6)$$

Then the bare quark mass is naturally added to the  $D_c$  in the numerator of (6),

$$D(m_q) = (D_c + m_q)(1 + raD_c)^{-1} . \quad (7)$$

Thus the quark propagator is

$$(D_c + m_q)^{-1} = (1 - rm_q a)^{-1} [D^{-1}(m_q) - ra] , \quad (8)$$

which is chirally symmetric in the massless limit. This exact chiral symmetry is the crucial feature one would like to preserve for any quark coupling to physical hadrons [11].

Then the pion propagator can be written as

$$M(\vec{x}, t; \vec{0}, 0) = \text{tr}\{\gamma_5(D_c + m_q)^{-1}(0, x)\gamma_5(D_c + m_q)^{-1}(x, 0)\} , \quad (9)$$

where the trace  $\text{tr}$  runs over Dirac and color space. Note that any one of the quark propagators in (9) can form the  $\eta'$  loop which leads to the quenched chiral logarithm in the pion mass as well as the condensate.

With the pion propagators, one can compute its time correlation function

$$G(t) = \sum_{\vec{x}} M(\vec{x}, t; \vec{0}, 0) , \quad (10)$$

which can then be fitted by the usual formula

$$G_\pi(t) = \frac{Z}{2m_\pi a} [e^{-m_\pi a t} + e^{-m_\pi a (T-t)}] , \quad (11)$$

to extract pion mass  $m_\pi a$ , and pion decay constant,

$$f_\pi a = 2m_q a \frac{\sqrt{Z}}{m_\pi^2 a^2} . \quad (12)$$

Besides the exact chiral symmetry, we also require that  $iD_c$  is hermitian, similar to the Dirac operator  $i\gamma_\mu(\partial_\mu + iA_\mu)$  in continuum. Then we have  $D_c^\dagger = \gamma_5 D_c \gamma_5$ . As a consequence of hermiticity and chiral symmetry, both quark propagators in (9) can be expressed in terms of that propagating from  $(\vec{0}, 0)$  to  $(\vec{x}, t)$ , i.e.,

$$\begin{aligned} M(\vec{x}, t; \vec{0}, 0) &= \text{tr}\{[(D_c + m_q)^{-1}(0, x)]^\dagger (D_c + m_q)^{-1}(x, 0)\} \\ &= \sum_{a,b=1}^3 \sum_{\alpha,\beta=1}^4 [(D_c + m_q)^{-1}{}_{a\alpha}{}^{b\beta}(x, 0)]^* (D_c + m_q)^{-1}{}_{a\alpha}{}^{b\beta}(x, 0) \end{aligned} \quad (13)$$

where  $a, b$  denote color indices, and  $\alpha, \beta$  Dirac indices. In other words, to obtain the time correlation function (10) of pion, one only needs to compute 12 columns of the matrix  $(D_c + m_q)^{-1}$ .

## 2.2 Practical implementation for overlap Dirac quark

The massless overlap Dirac operator [6] reads as

$$D = m_0 a^{-1} \left( \mathbb{1} + \gamma_5 \frac{H_w}{\sqrt{H_w^2}} \right) \quad (14)$$

where  $H_w$  denotes the hermitian Wilson-Dirac operator with a negative parameter  $-m_0$ ,

$$H_w = \gamma_5 D_w = \gamma_5 (-m_0 + \gamma_\mu t_\mu + W) , \quad (15)$$

$\gamma_\mu t_\mu$  the naive fermion operator, and  $W$  the Wilson term. Then  $D$  (14) satisfies the Ginsparg-Wilson relation (5) with  $r = 1/(2m_0)$ . Note that the value of  $m_0$  has to be chosen properly such that the overlap Dirac operator can capture the topology of the gauge configuration, as well as behaving like a massless Dirac fermion even in a topologically trivial gauge background. In other words, on a finite lattice, the proper range of  $m_0$  for any gauge configuration is smaller than that ( $0 < m_0 < 2$ ) in the free fermion limit. However, one usually does not need to finely tune  $m_0$  except for rough gauge configurations at strong couplings [12]. In this paper, we fix  $m_0 = 1.3$  for our computations.

Now the difficult task is to compute the quark propagator with exact chiral symmetry (8), which amounts to computing

$$D^{-1}(m_q) = D^\dagger(m_q) \{D(m_q) D^\dagger(m_q)\}^{-1} ,$$

where the positive hermitian operator  $D(m_q)D^\dagger(m_q)$  can be written as

$$D(m_q)D^\dagger(m_q) = \left[ m_q^2 + \left( m_0^2 - \frac{m_q^2}{4} \right) \left( 2 + \gamma_5 \frac{H_w}{\sqrt{H_w^2}} + \frac{H_w}{\sqrt{H_w^2}} \gamma_5 \right) \right]. \quad (16)$$

Then the quark propagators from the reference point  $(\vec{0}, 0)$  to all sites  $(\vec{x}, t)$  can be obtained by solving 12 column vectors  $Y_{c\alpha}(\vec{x}, t)$  ( where  $c$  and  $\alpha$  are color and Dirac indices of the quark field at  $(\vec{0}, 0)$  ) in the following linear system for 12 point source vectors on the r.h.s.,

$$D(m_q)D^\dagger(m_q)Y_{c\alpha}(\vec{x}, t) = \mathbb{1}_{c\alpha}, \quad (17)$$

where  $D(m_q)D^\dagger(m_q)$  is expressed by (16). Due to the rather small size of the physical memory in the present generation of computers, the viable ways to solve the linear system (17) are iterative methods, in which the conjugate gradient algorithm is the most optimal for positive definite matrices. Starting from an initial guess of  $Y^{(0)}$ , we multiply  $DD^\dagger$  to  $Y^{(0)}$ , and update  $Y^{(0)}$  to  $Y^{(1)}$  according to the conjugate gradient algorithm, then iterate this process until  $Y^{(n)}$  converges to the solution with desired accuracy  $\epsilon$ , i.e.,

$$\|D(m_q)D^\dagger(m_q)Y_{c\alpha}^{(n)}(\vec{x}, t) - \mathbb{1}_{c\alpha}\| < \epsilon. \quad (18)$$

In this paper, we set  $\epsilon = 10^{-11}$ .

Now the updating process involves the multiplication of the matrix

$$\frac{1}{\sqrt{H_w^2}} \quad (19)$$

to the vector  $Y^{(i)}$ . However, (19) does not have analytic closed form. This is the major challenge for lattice QCD with overlap Dirac quark. A way to proceed is to express (19) in terms of a rational approximation [13]

$$\frac{1}{\sqrt{H_w^2}} \simeq \sum_{l=1}^k \frac{b_l}{H_w^2 + d_l}, \quad (20)$$

where  $b_l$  and  $d_l$  are some positive definite coefficients. Then the matrix-vector multiplication

$$\frac{1}{\sqrt{H_w^2}} Y^{(i)} \simeq \sum_{l=1}^k \frac{b_l}{H_w^2 + d_l} Y^{(i)} = \sum_{l=1}^k b_l Z_l$$

can be evaluated by invoking another conjugate gradient process to the linear systems

$$(H_w^2 + d_l)Z_l = Y^{(i)}, \quad l = 1, \dots, k. \quad (21)$$

Instead of solving each  $Z_l$  individually, one can use multi-shift CG algorithm [14], and obtain all  $Z_l$  altogether, with only a small fraction of the total time what one had computed each  $Z_l$  separately. Evidently, one can also apply multi-shift CG algorithm to (17) to obtain several quark propagators with different bare quark masses.

Now the computation of overlap Dirac quark propagator involves two nested conjugate gradient loops : the so-called inner CG loop (21), and the outer CG loop (17). The inner CG loop is the price what one pays for preserving the exact chiral symmetry at finite lattice spacing.

The computational cost can be saved more than 50% by observing that  $D(m_q)D^\dagger(m_q)$  (16) commutes with  $\gamma_5$ . Thus one can choose chiral sources on the r.h.s. of (17),

$$(\mathbb{I}_{c\alpha})^{b\beta}(\vec{x}, t) = \delta_{cb}\delta_{\alpha\beta} p(\vec{x}, t)$$

where  $p(\vec{x}, t) = \delta_{\vec{x},\vec{0}}\delta_{t,0}$  for a point source. Then we have

$$\begin{aligned}\gamma_5 \mathbb{I}_{c\alpha} &= +\mathbb{I}_{c\alpha}, & \alpha = 1, 2, \\ \gamma_5 \mathbb{I}_{c\alpha} &= -\mathbb{I}_{c\alpha}, & \alpha = 3, 4,\end{aligned}$$

and

$$\begin{aligned}\gamma_5 Y_{c\alpha} &= +Y_{c\alpha}, & \alpha = 1, 2, \\ \gamma_5 Y_{c\alpha} &= -Y_{c\alpha}, & \alpha = 3, 4.\end{aligned}$$

Now one of the two matrix-vector multiplications in the outer CG loop can be eliminated, since the l.h.s. of (17) becomes

$$D(m_q)D^\dagger(m_q)Y_{c\alpha} = \left\{ m_q^2 + \left( 2m_0^2 - \frac{m_q^2}{2} \right) \left[ 1 + \frac{(\gamma_5 \pm 1)}{2} H_w \frac{1}{\sqrt{H_w^2}} \right] \right\} Y_{c\alpha} \quad (22)$$

where '+' for  $\alpha = 1, 2$ , and '-' for  $\alpha = 3, 4$ . Further, due to the projector  $(\gamma_5 \pm 1)/2$ , half of the matrix-vector multiplication in

$$H_w \cdot \frac{1}{\sqrt{H_w^2}} Y_{c\alpha}$$

can be saved.

The next crucial question is how to fix the values of coefficients  $b_l$  and  $d_l$  in (20) such that the inverse square root function can be approximated optimally. Fortunately, this problem has been solved by Zolotarev [15] in 1877, using Jacobian elliptic functions. A comparative study of Zolotarev's optimal rational approximation versus other schemes for the overlap Dirac operator has been reported in Ref. [16].

For the inverse square root function

$$\frac{1}{\sqrt{x}}, \quad x \in [1, x_{max}] , \quad (23)$$

the Zolotarev optimal rational approximation is

$$f(x) = d_0 \frac{\prod_{l=1}^{k-1} (x + c_{2l})}{\prod_{l=1}^k (x + c_{2l-1})} \quad (24)$$

where

$$c_l = \frac{\operatorname{sn}^2(lK/2k; \kappa)}{1 - \operatorname{sn}^2(lK/2k; \kappa)}, \quad \kappa = \sqrt{1 - 1/x_{max}} , \quad (25)$$

the Jacobian elliptic function  $\operatorname{sn}(u, \kappa) = \eta$  is defined by the elliptic integral

$$u(\eta) = \int_0^\eta \frac{dt}{\sqrt{(1-t^2)(1-\kappa^2 t^2)}} , \quad (26)$$

$K = u(1)$  is the complete elliptic integral, and  $d_0$  is uniquely determined by the condition

$$\max[1 - \sqrt{x}f(x)]|_{x \in [1, x_{max}]} = -\min[1 - \sqrt{x}f(x)]|_{x \in [1, x_{max}]}$$

For our purpose, it suffices to fix  $d_0$  such that  $f(1) = 1$ .

Since the eigenvalues of  $H_w$  are bounded,

$$\lambda_{min} \leq |\lambda(H_w)| \leq \lambda_{max} , \quad (27)$$

we can rescale  $H_w$ ,

$$h_w \equiv H_w / \lambda_{min} , \quad (28)$$

such that the eigenvalues of  $h_w^2$  fall inside the interval  $[1, (\lambda_{max}/\lambda_{min})^2]$ .

After obtaining the partial fraction of (24), we have the optimal rational approximation to the inverse square root of  $H_w^2$

$$\frac{1}{\sqrt{H_w^2}} \simeq \frac{1}{\lambda_{min}} \sum_{l=1}^k \frac{b_l}{h_w^2 + d_l} \quad (29)$$

where

$$d_l = c_{2l-1} , \quad (30)$$

$$b_l = d_0 \frac{\prod_{i=1}^{k-1} (c_{2i} - c_{2l-1})}{\prod_{i=1, i \neq l}^k (c_{2i-1} - c_{2l-1})} , \quad (31)$$



and the parameter  $\kappa$  in the Jacobian elliptic function  $\text{sn}(lK/2k; \kappa)$  is

$$\kappa = \sqrt{1 - (\lambda_{min}/\lambda_{max})^2} . \quad (32)$$

Note that, for a given order  $k$ , the smaller the interval  $[1, (\lambda_{max}/\lambda_{min})^2]$ , the more accurate the rational approximation is. Thus, it is advantageous to narrow the interval  $[\lambda_{min}, \lambda_{max}]$  by projecting out the eigenmodes at both ends. Since the spectrum of  $H_w^2$  is very dense near the upper bound, we only need to project out one or two eigenmodes near  $\lambda_{max}$ , just to get the precise value of  $\lambda_{max}$ . On the other hand, we usually project out 20 or more low-lying eigenmodes of  $H_w^2$ , such that  $(\lambda_{max}/\lambda_{min})^2$  is always less than 2500. Then we project the inner CG loop to the complement of the vector space spanned by these eigenmodes. This not only gives a better rational approximation for the inverse square root of  $H_w^2$ , but also reduces the number of iterations of the inner CG loop, which is proportional to the condition number  $(\lambda_{max}/\lambda_{min})^2$ .

We use Arnoldi algorithm to compute a selected subset of eigenmodes of  $H_w$ , which correspond to high and low lying ones of  $H_w^2$ . Denoting these eigenmodes by

$$H_w u_j = \lambda_j u_j, \quad j = 1, \dots, n , \quad (33)$$

we project the inner CG loop (21) to the complement of the vector space spanned by these eigenmodes ( i.e., multiplying both sides of (21) by the projector  $P = 1 - \sum_{j=1}^n u_j u_j^\dagger$ , and use  $PH_w = H_w P$  ),

$$(h_w^2 + d_l)\bar{Z}_l = \bar{Y}^{(i)} \equiv (1 - \sum_{j=1}^n u_j u_j^\dagger)Y^{(i)} . \quad (34)$$

Note that  $\lambda_{min}$  and  $\lambda_{max}$  in Eqs. (27)-(32) now refer to upper and lower bounds of  $|\lambda(\bar{H}_w)|$ , where

$$\bar{H}_w = PH_w = H_w - \sum_{j=1}^n \lambda_j u_j u_j^\dagger . \quad (35)$$

Then the matrix-vector multiplication at each step of outer CG loop can be expressed in terms of the projected eigenmodes (33) plus the solution obtained from the inner CG loop (34) in the complementary vector space, i.e.,

$$H_w \frac{1}{\sqrt{H_w^2}} Y^{(i)} \simeq \frac{1}{\lambda_{min}} \bar{H}_w \sum_{l=1}^k b_l \bar{Z}_l + \sum_{j=1}^n \frac{\lambda_j}{\sqrt{\lambda_j^2}} u_j u_j^\dagger Y^{(i)} \equiv S^{(i)} . \quad (36)$$

The accuracy of  $S^{(i)}$  can be measured by the deviation

$$\sigma_i = \frac{|S^{(i)\dagger} S^{(i)} - Y^{(i)\dagger} Y^{(i)}|}{Y^{(i)\dagger} Y^{(i)}} , \quad (37)$$

which would be zero if (36) is exact.

In this paper, we project out 20 lowest-lying and 4 largest eigenmodes of  $H_w^2$ , and use 20 terms ( $k = 20$ ) in the Zolotarev optimal rational approximation, and set the convergence criterion for inner CG loop to  $10^{-12}$ , then  $\sigma_i$  is always less than  $10^{-11}$  for any iteration of the outer CG loop.

## 2.3 Results

With the Wilson  $SU(3)$  gauge action at  $\beta = 5.8$ , we generate 100 gauge configurations on the  $8^3 \times 24$  lattice, using Creutz-Cabibbo-Marinari heat bath algorithm [23, 24]. For each configuration, we compute quenched quark propagators for 12 bare quark masses. Then the pion propagator (13) and its time correlation functions (10) are obtained, and the latter are fitted by (11) to yield the pion mass  $m_\pi a$  and decay constant  $f_\pi a$ .

In Figs. 1 and 2, we plot the pion mass square  $(m_\pi a)^2$  and decay constant  $f_\pi a$  versus the bare quark mass  $m_q a$  respectively. The data of  $f_\pi a$  can be fitted by

$$f_\pi a = 0.0984(3) + 0.1635(15)(m_q a) \quad (38)$$

with  $\chi^2/d.o.f. = 0.03$ . Now we take the value  $f_\pi a = 0.0984(3)$  at  $m_q a = 0$  equal to the experimental value of pion decay constant  $f_\pi = 132$  MeV times the lattice spacing  $a$ ,

$$f_\pi a = 0.0984(3) = 132 \text{ MeV} \times a, \quad (39)$$

then this gives an estimate of the lattice spacing

$$a = 0.147(1) \text{ fm} . \quad (40)$$

Thus the lattice size is  $\sim (1.2 \text{ fm})^3 \times 3.5 \text{ fm}$ . Since the smallest pion mass is  $\sim 418$  MeV, the lattice size is  $\sim (2.5)^3 \times 7.5$ , in units of the Compton wavelength ( $\sim 0.47$  fm) of the lowest-mass pion.

Fixing the cutoff  $\Lambda_\chi = 2\sqrt{2}\pi f_\pi$  as in quenched chiral perturbation theory (i.e.,  $\Lambda_\chi a = 2\sqrt{2}\pi f_\pi a = 0.8745$ ), we fit (1) to our data of  $(m_\pi a)^2$ , and obtain

$$\delta = 0.2034(140), \quad (41)$$

$$Ca = 1.1932(182), \quad (42)$$

$$B = 1.1518(556), \quad (43)$$

with  $\chi^2/d.o.f. = 0.03$ .

Even though one may not easily detect the quenched chiral logarithm in Fig. 1, it can be unveiled by plotting  $(m_\pi a)^2/(m_q a)$  versus  $m_q a$ , as shown in Fig. 3. Further, we can subtract the quadratic term  $Bm_q^2$  [with the value of  $B$  given in (43)], and check its dependence on  $\ln(m_q)$  explicitly. In Fig 4,

we plot  $(m_\pi a)^2/(m_q a) - B(m_q a)$  versus  $\log(m_q a)$ . The presence of quenched chiral logarithm is evident.

In passing, we note that a finite lattice must impose a lower bound for the pion mass, as well as the corresponding one for the bare quark mass. If one decreases the bare quark mass beyond its lower bound, then the resulting pion mass would be flattening ( or increasing ) rather than decreasing. This is essentially due to the finite volume effects of the zero modes of the overlap Dirac operator in the pion propagator, which is proportional to  $|n_+ - n_-|/(m_q^2 a^2 N_s)$  as  $m_q a \rightarrow 0$ . Thus, only in the infinite volume limit (  $N_s \rightarrow \infty$  ), one can obtain zero pion mass with zero bare quark mass. Nevertheless, for a finite lattice, the finite volume effects of the zero modes can be suppressed if the bare quark mass  $m_q a \gg \sqrt{|n_+ - n_-|/N_s}$ . For a lattice of size  $8^3 \times 24$  at  $\beta = 5.8$ , we find that  $m_q a \geq 0.06$  is sufficient to suppress the finite volume effects of the zero modes. This can be verified by comparing the results (41)-(43) to those obtained in larger volumes, e.g.,  $12^3 \times 24$  at  $\beta = 5.8$  ( which is about 3.4 times of the present volume ). Another plausible check is to see whether the  $\delta$  extracted from the pion mass agrees with that obtained from the index susceptibility, Eq.(4), since the index susceptibility and the  $f_\pi a$  ( see Fig. 2 ) both presumably suffer the least from the finite volume effects. The latter check is performed in Section 3, and the agreement between these two  $\delta$ 's suggests that the finite volume effects may be under control.

### 3 Index susceptibility and the $\eta'$ mass

In this section, we derive a relationship between the index susceptibility of any Ginsparg-Wilson lattice Dirac operator and the  $\eta'$  mass as depicted in quenched chiral perturbation theory. Then we measure the index of overlap Dirac operator for those 100 gauge configurations used for computing quark propagators in Section 2, and obtain the index susceptibility, the  $\eta'$  mass, and an estimate of  $\delta = 0.197 \pm 0.027$ , which is in good agreement with the  $\delta$  determined from the pion mass in Section 2.

#### 3.1 A formula due to exact chiral symmetry

The propagator of ( flavor-singlet )  $\eta'$  can be written as

$$M_{\eta'}(x, y) = \text{tr}\{\gamma_5(D_c + m_q)^{-1}(y, x)\gamma_5(D_c + m_q)^{-1}(x, y)\} - \text{tr}\{\gamma_5(D_c + m_q)^{-1}(y, y)\}\text{tr}\{\gamma_5(D_c + m_q)^{-1}(x, x)\} \quad (44)$$

where the second term on r.h.s. is the commonly called hairpin diagram. Note that the first term is just the usual pion propagator (9), while the second term can be regarded as pion propagator with the  $\eta'$  mass insertion due to the

nontrivial interactions of gluons between two seemingly disconnected quark propagators.

In the quenched approximation, the expectation value of the hairpin diagram in momentum space can be written as

$$\begin{aligned} & \left\langle \frac{1}{V} \sum_{x,y} e^{ip \cdot (x-y)} \text{tr}\{\gamma_5(D_c + m_q)^{-1}(y, y)\} \text{tr}\{\gamma_5(D_c + m_q)^{-1}(x, x)\} \right\rangle \\ &= \sqrt{Z} \frac{1}{p^2 + m_\pi^2} m_{\eta'}^2 \frac{1}{p^2 + m_\pi^2} \sqrt{Z} \end{aligned} \quad (45)$$

where the brackets  $\langle \dots \rangle$  denote quenched average over gauge configurations with weight  $e^{-\mathcal{A}_g}$  ( $\mathcal{A}_g$  : pure gauge action), and

$$\sqrt{Z} = \frac{m_\pi^2 f_\pi}{2m_q}$$

as defined in (11) and (12). Equation (45) can be regarded as the definition of the  $\eta'$  mass in quenched chiral perturbation theory.

At zero momentum  $p = 0$ , (45) becomes

$$\left\langle \frac{1}{V} \sum_{x,y} \text{tr}\{\gamma_5(D_c + m_q)^{-1}(y, y)\} \text{tr}\{\gamma_5(D_c + m_q)^{-1}(x, x)\} \right\rangle = \frac{f_\pi^2 m_{\eta'}^2}{4m_q^2} \quad (46)$$

Now the expression inside the brackets  $\langle \dots \rangle$  can be evaluated exactly in terms of the index of  $D_c$  ( $D$ ). Explicitly,

$$\begin{aligned} & \sum_x \text{tr}\{\gamma_5(D_c + m_q)^{-1}(x, x)\} = \text{Tr}\{\gamma_5(D_c + m_q)^{-1}\} \\ &= (1 - rm_q a)^{-1} \sum_\alpha \phi_\alpha^\dagger \gamma_5 \phi_\alpha \{[m_q + (1 - rm_q a)\lambda_\alpha]^{-1} - ra\} \end{aligned} \quad (47)$$

where (7) and (8) have been used, and the trace Tr is evaluated in terms of the eigenvalues  $\{\lambda_\alpha\}$  and eigenvectors  $\{\phi_\alpha\}$  of the Ginsparg-Wilson lattice Dirac operator  $D$  (6) with  $D_c$  satisfying  $(iD_c)^\dagger = iD_c$ . Recalling the properties of the eigensystem of  $D$  [17],

$$\phi_\alpha^\dagger \gamma_5 \phi_\alpha = \begin{cases} 0 & \text{for } \lambda_\alpha \neq \lambda_\alpha^* \\ \pm 1 & \text{for } \lambda_\alpha = \lambda_\alpha^* \end{cases}$$

one immediately sees that only the real eigenmodes  $\lambda = 0$  and  $(ra)^{-1}$  can contribute to (47). Since the factor  $\{[m_q + (1 - rm_q a)\lambda_\alpha]^{-1} - ra\}$  vanishes for  $\lambda_\alpha = (ra)^{-1}$ , thus only the zero modes contribute to (47), i.e.,

$$\sum_x \text{tr}\{\gamma_5(D_c + m_q)^{-1}(x, x)\} = \frac{n_+ - n_-}{m_q}. \quad (48)$$

Substituting (48) into l.h.s. of (46), one obtains

$$N_f \frac{\langle (n_+ - n_-)^2 \rangle}{V} = \frac{f_\pi^2 m_{\eta'}^2}{4}, \quad (49)$$

where the factor  $N_f$  denotes the number of light quark flavors, which accounts for the number of hairpin diagrams contributing to the  $\eta'$  mass. Since (49) is an exact result following from the definition of  $m_{\eta'}$  in (45), it offers the best way to obtain the  $\eta'$  mass in quenched chiral perturbation theory. One just measures the index (susceptibility) of the Ginsparg-Wilson lattice Dirac operator, without computing the hairpin diagram at all. This is one of the advantages of preserving exact chiral symmetry on the lattice. Note that (49) is independent of the bare quark mass  $m_q$ , thus the  $\eta'$  can remain massive even in the limit  $m_q \rightarrow 0$ . This is the crucial feature of the  $\eta'$  to distinguish itself from the octet of approximate Goldstone bosons, the  $\pi$ ,  $K$  and  $\eta$ .

Recently, (49) is derived [20] differently starting from the anomalous flavor-singlet axial Ward identity, which is formally equivalent to replacing the continuum topological charge density  $\rho$  in the Witten-Veneziano formula [18, 19]

$$m_{\eta'}^2 = \frac{4N_f}{f_\pi^2} \int d^4x \langle \rho(x) \rho(0) \rangle, \quad \rho = \frac{1}{32\pi^2} \epsilon_{\mu\nu\lambda\sigma} \text{tr}(F_{\mu\nu} F_{\lambda\sigma}), \quad (50)$$

with the axial anomaly  $q = \text{tr}[\gamma_5(1 - raD)]$  of the overlap Dirac operator, and the integration  $\int d^4x$  with the summation over all sites  $\sum_x$ . That is, the integral in (50) is formally transcribed as

$$\int d^4x \langle \rho(x) \rho(0) \rangle \iff a^{-4} \sum_x \langle q(x) q(0) \rangle. \quad (51)$$

Since (50) is derived in the large  $N_c$  limit (which is valid to lowest order in  $1/N_c$ ), a relevant question is what value of  $N_c$  in Eq. (50) is supposed to be valid. Further, even though the r.h.s. of (51) is well-defined on a finite lattice, some subtleties [21] could emerge as the 2-point function  $\langle q(x) q(0) \rangle$  ( $x \neq 0$ ) becomes non-positive in the continuum limit, since  $\rho(x)$  is odd under time reflections. Thus, a real  $m_{\eta'}$  would require a divergent contact term  $\langle \rho^2(0) \rangle$ . How to fix this contact term is the basic problem of Witten-Veneziano formula (50) in the continuum. On the other hand, for a finite lattice, one can use the well-known relation  $\sum_x q(x) = n_+ - n_-$  to turn the r.h.s. of (51) into the index susceptibility,

$$a^{-4} \sum_x \langle q(x) q(0) \rangle = \frac{1}{V} \sum_x \sum_y \langle q(x) q(y) \rangle = \frac{1}{V} \langle (n_+ - n_-)^2 \rangle, \quad (52)$$

which is well-defined in the limit  $V \rightarrow \infty$  and  $a \rightarrow 0$ . Nevertheless, it is still interesting to see whether  $\langle q(x) q(0) \rangle$  ( $x \neq 0$ ) would become negative in the continuum limit, together with a divergent contact term.

It should be emphasized that our derivation of (49) is quite different from that of Ref. [20]. We start from Eq. (45) which serves as the definition of the  $\eta'$  mass in quenched chiral perturbation theory. Then the subsequent steps leading to (49) are exact due to chiral symmetry, without any approximations or assumptions. This is in contrast to the approach used in Ref. [20], in which the anomalous flavor-singlet axial Ward identity is used, in the limit  $u \equiv N_f/N_c \rightarrow 0$ . The subtleties arising from  $\langle q(x)q(0) \rangle$  in the continuum limit cannot be resolved unless one transcribes the expression in terms of the index susceptibility of a Ginsparg-Wilson lattice Dirac operator. Finally we note that a derivation of (49) similar to our approach is also presented in Ref. [22] for the overlap Dirac operator.

### 3.2 Measurement of the index of the overlap

The index of overlap Dirac operator (14) is

$$\text{index}(D) = \sum_x \text{tr}[\gamma_5(1 - arD(x, x))] = \frac{1}{2}(h_- - h_+) \quad (53)$$

where  $h_+(h_-)$  is the number of positive ( negative ) eigenvalues of the hermitian Wilson-Dirac operator  $H_w$  (15). However, one does not need to obtain all eigenvalues of  $H_w$  in order to know how many of them are positive or negative. The idea is simple. Since  $H_w$  has equal number of positive and negative eigenvalues for  $m_0 \leq 0$ , then one can just focus at those low-lying ( near zero ) eigenmodes of  $H_w$ , and see whether any of them crosses zero from positive to negative, or vice versa, when  $m_0$  is scanned from 0 up to the value ( e.g., 1.30 in this paper ) used in the definition of  $D$ . From the net number of crossings, one can obtain the index of  $D$  (53). This is the spectral flow method used in Refs. [7, 25] to obtain the index of overlap Dirac operator.

In Fig. 5, we plot the spectral flow of eight lowest-lying ( near zero ) eigenvalues of  $H_w(m_0)$  in the interval  $0.9 \leq m_0 \leq 1.3$ , for one of the gauge configurations. Evidently, the flows are not as smooth as one may have expected. In this case, the net crossings is -6 ( from negative to positive ), so the index of the overlap Dirac operator is -6. In some cases ( see, for example, Fig 6 ), there are some intriguing eigenvalues lying very close to zero, thus for a coarse scan in  $m_0$ , it may not be so easy to determine whether they actually cross zero or not. These ambiguities can only be resolved by tracing them closely at a finer resolution in  $m_0$ .

The distribution of the indices of  $D$  for these 100 gauge configurations is listed in Table 1. So the index susceptibility is

$$a^4\chi = \frac{\langle (n_+ - n_-)^2 \rangle}{N_s} = 3.67(50) \times 10^{-4} \quad (54)$$

$I = n_+ - n_-$	number of configurations
4	2
3	11
2	9
1	14
0	24
-1	15
-2	11
-3	6
-4	6
-5	1
-6	1

Table 1: The distribution of the indices of overlap Dirac operator for 100 gauge configurations at  $\beta = 5.80$  on the  $8^3 \times 24$  lattice. Here  $\langle I \rangle = -0.19$  and  $\langle I^2 \rangle = 4.51$ .

where  $N_s$  is the total number of sites. Now if we subtract the mean value  $\langle n_+ - n_- \rangle = -0.19$  from all indices, then the index susceptibility becomes

$$a^4 \chi = \frac{\langle (n_+ - n_-)^2 \rangle - \langle n_+ - n_- \rangle^2}{N_s} = 3.64(50) \times 10^{-4} \quad (55)$$

Now substitute the index susceptibility (55), the lattice spacing (40),  $f_\pi = 132$  MeV, and  $N_f = 3$ , into the exact relation (49), we obtain the  $\eta'$  mass

$$m_{\eta'} = (901 \pm 64) \text{MeV} , \quad (56)$$

which agrees with the theoretical estimate

$$\sqrt{\mathbf{m}_{\eta'}^2 + m_\eta^2 - 2m_K^2} = 853 \text{ MeV} , \quad (57)$$

with experimental values of meson masses<sup>1</sup> :  $\mathbf{m}_{\eta'} = 958$  MeV,  $m_\eta = 547$  MeV, and  $m_K = 495$  MeV.

Next we substitute (55) and  $f_\pi a = 0.0984(3)$  into (4), and get

$$\delta = 0.197 \pm 0.027 , \quad (58)$$

which is in good agreement with the value (41) determined from the pion mass, as well as with the theoretical estimate  $\delta \simeq 0.2$ .

---

<sup>1</sup>Here we distinguish the physical  $\eta'$  mass ( $\mathbf{m}_{\eta'}$ ), from the  $\eta'$  mass ( $m_{\eta'}$ ) in quenched chiral perturbation theory.

## 4 Concluding remarks

In this paper, we have examined the quenched chiral logarithm in lattice QCD with overlap Dirac quark. The coefficient of quenched chiral logarithm ( $\delta = 0.203 \pm 0.014$ ) extracted from the pion mass agrees very well with that ( $\delta = 0.197 \pm 0.027$ ) obtained from the index susceptibility of overlap Dirac operator. Further, they are in good agreement with the theoretical estimate  $\delta \simeq 0.2$  in quenched chiral perturbation theory. This provides strong evidences that lattice QCD with overlap Dirac quark realizes quenched QCD chiral dynamics, as depicted by quenched chiral perturbation theory.

Our results on pion mass and decay constant rely very much on the viability of computing quark propagators to a high accuracy. We find that the accuracy in the implementation of the inverse square root of  $H_w^2$  is the most crucial step in this two-level conjugate gradient paradigm. The Zolotarev optimal rational approximation together with projection of high and low-lying eigenmodes enables us to control the error of  $\text{sign}(H_w)Y$  always less than  $10^{-11}$ , at each iteration of the outer CG loop. The details of our implementation are described in Section 2.

Equation (49) is an exact result following from the definition of the  $\eta'$  mass in (45). It provides the best way to obtain the  $\eta'$  mass in quenched chiral perturbation theory, as well as to determine the coefficient of quenched chiral logarithm in terms of the index susceptibility of any topologically-proper Ginsparg-Wilson lattice Dirac operator. Equation (4) may even suggest that  $\delta$  is scale invariant for a range of lattice spacings including the continuum limit  $a \rightarrow 0$ . This also explains why the  $\delta$  value we obtained at  $a = 0.147$  fm is so close to the theoretical estimate in the continuum.

At this point, it may be interesting to recall an example of lattice Dirac operator with exact chiral symmetry [26]. Unlike the overlap Dirac operator, it does not have topological zero modes for any nontrivial gauge backgrounds. However, it reproduces correct axial anomaly in the continuum limit [27], at least for the trivial gauge sector. Since its index is zero, its index susceptibility must be zero, and it follows that the  $\eta'$  mass is zero, and the quenched chiral logarithm is absent in the pion mass as well as other related quantities. Nevertheless, it does not necessarily imply that this lattice Dirac operator could not be realized in nature. It seems that the real testing ground for this lattice Dirac operator is lattice QCD with dynamical quarks, in which all quenched pathologies are absent.

In passing, we briefly outline the essential features of our computing system. The platform is a home-made Linux PC cluster with 18 nodes, built with off-the-shelf components. Each node consists of one Pentium 4 processor ( 1.6 Ghz ) with one Gbyte of Rambus, one 40 Gbyte hard disk, and a network card. The computational intensive parts ( matrix-vector operations ) of our program are written in SSE2 codes [28], which can double the speed of our earlier



pure Fortran codes compiled by Intel Fortran Compiler 5.0 with maximum optimizations including the SSE2 option. The performance of our system is estimated to be around 20 Gflops.

This work was supported in part by the National Science Council, ROC, under the grant number NSC90-2112-M002-021, and also in part by NCTS.

## References

- [1] S. R. Sharpe, Phys. Rev. D **46**, 3146 (1992)
- [2] C. W. Bernard and M. F. Golterman, Phys. Rev. D **46**, 853 (1992)
- [3] S. Aoki *et al.* [CP-PACS Collaboration], Phys. Rev. Lett. **84**, 238 (2000)
- [4] W. Bardeen, A. Duncan, E. Eichten and H. Thacker, Phys. Rev. D **62**, 114505 (2000)
- [5] C. W. Bernard *et al.*, Phys. Rev. D **64**, 054506 (2001)
- [6] H. Neuberger, Phys. Lett. B **417**, 141 (1998);
- [7] R. Narayanan and H. Neuberger, Nucl. Phys. B **443**, 305 (1995)
- [8] S. J. Dong, T. Draper, I. Horvath, F. X. Lee, K. F. Liu and J. B. Zhang, Phys. Rev. D **65**, 054507 (2002)
- [9] P. H. Ginsparg and K. G. Wilson, Phys. Rev. D **25**, 2649 (1982).
- [10] T. W. Chiu and S. V. Zenkin, Phys. Rev. D **59**, 074501 (1999)
- [11] T. W. Chiu, Phys. Rev. D **60**, 034503 (1999)
- [12] T. W. Chiu, Phys. Rev. D **60**, 114510 (1999)
- [13] H. Neuberger, Phys. Rev. Lett. **81**, 4060 (1998)
- [14] A. Frommer, B. Nockel, S. Gusken, T. Lippert and K. Schilling, Int. J. Mod. Phys. C **6**, 627 (1995)
- [15] E. I. Zolotarev, “Application of elliptic functions to the questions of functions deviating least and most from zero”, Zap. Imp. Akad. Nauk. St. Petersburg, 30 (1877), no. 5; reprinted in his Collected works, Vol. 2, Izdat, Akad. Nauk SSSR, Moscow, 1932, p. 1-59.
- [16] J. van den Eshof, A. Frommer, T. Lippert, K. Schilling and H. A. van der Vorst, Nucl. Phys. Proc. Suppl. **106**, 1070 (2002)

- [17] T.W. Chiu, Phys. Rev. D **58**, 074511 (1998)
- [18] E. Witten, Nucl. Phys. B **156**, 269 (1979).
- [19] G. Veneziano, Nucl. Phys. B **159**, 213 (1979).
- [20] L. Giusti, G. C. Rossi, M. Testa and G. Veneziano, Nucl. Phys. B **628**, 234 (2002)
- [21] E. Seiler, Phys. Lett. B **525**, 355 (2002); E. Seiler and I. O. Stamatescu, MPI-PAE/PTh 10/87.
- [22] T. DeGrand and U. M. Heller [MILC collaboration], hep-lat/0202001.
- [23] M. Creutz, Phys. Rev. D **21** (1980) 2308.
- [24] N. Cabibbo and E. Marinari, Phys. Lett. B **119** (1982) 387.
- [25] R. G. Edwards, U. M. Heller and R. Narayanan, Nucl. Phys. B **535**, 403 (1998)
- [26] T. W. Chiu, Phys. Lett. B **521**, 429 (2001)
- [27] T. W. Chiu and T. H. Hsieh, Phys. Rev. D **65**, 054508 (2002)
- [28] M. Luscher, Nucl. Phys. Proc. Suppl. **106**, 21 (2002)

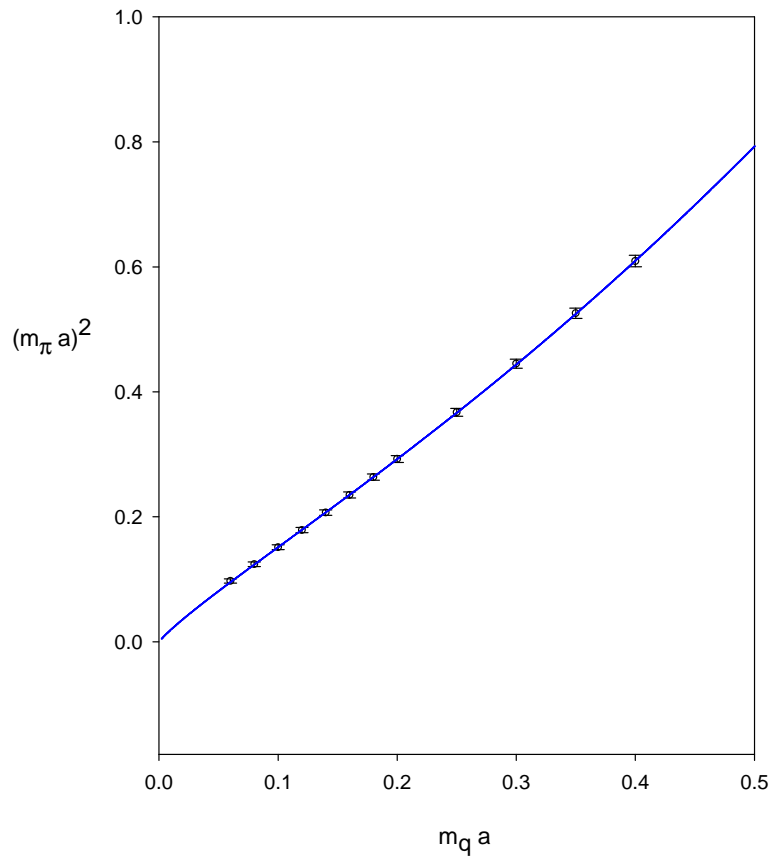


Figure 1: The pion mass square  $(m_\pi a)^2$  versus the bare quark mass  $m_q a$ . The solid line is the fit of Eq. (1).

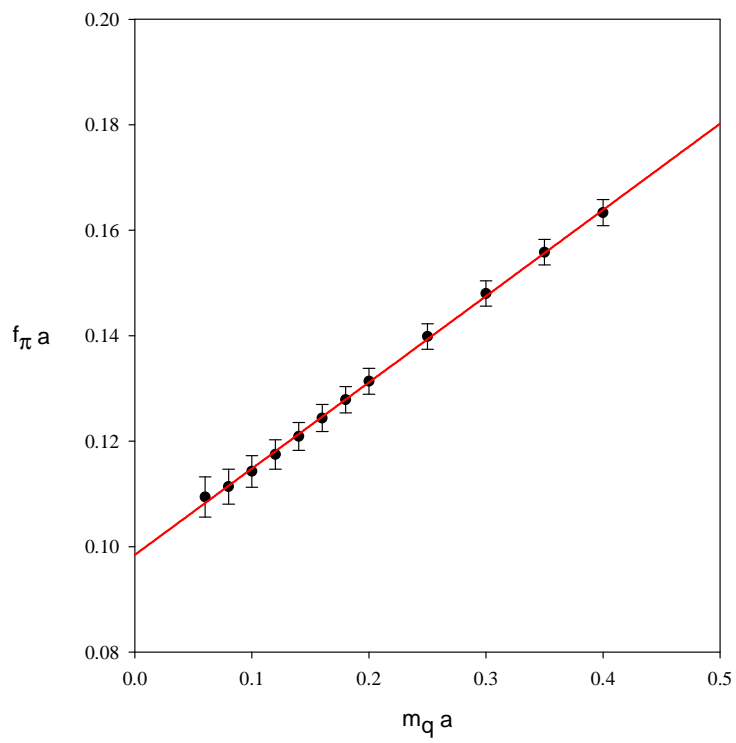


Figure 2: The pion decay constant  $f_\pi a$  versus the bare quark mass  $m_q a$ . The solid line is the linear fit.

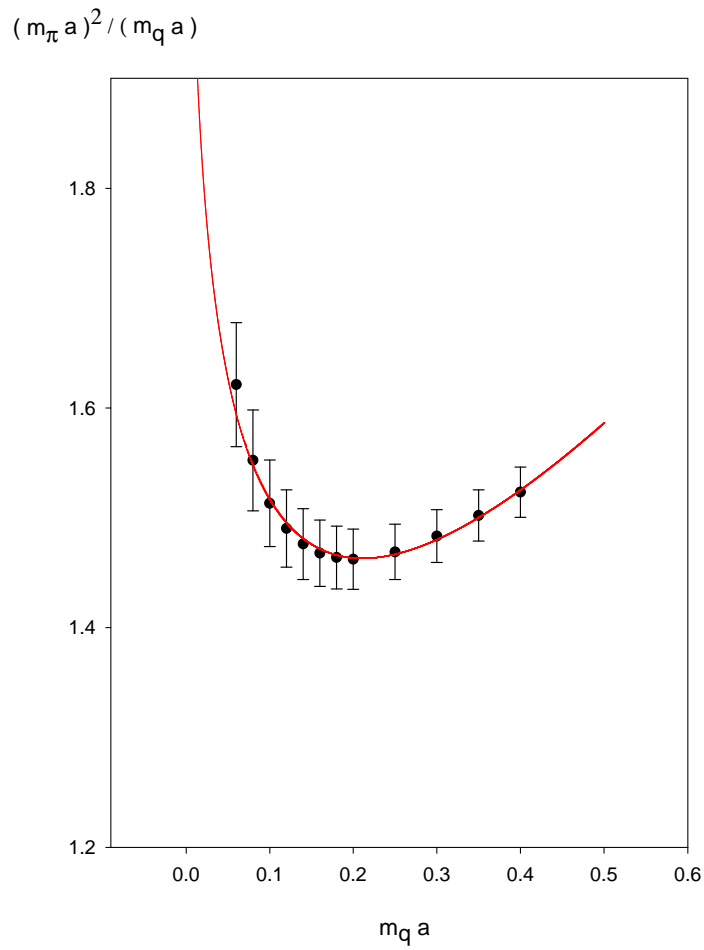


Figure 3:  $(m_\pi a)^2 / (m_q a)$  versus the bare quark mass  $m_q a$ . The solid line is the fit of Eq. (1) divided by  $m_q a$ .

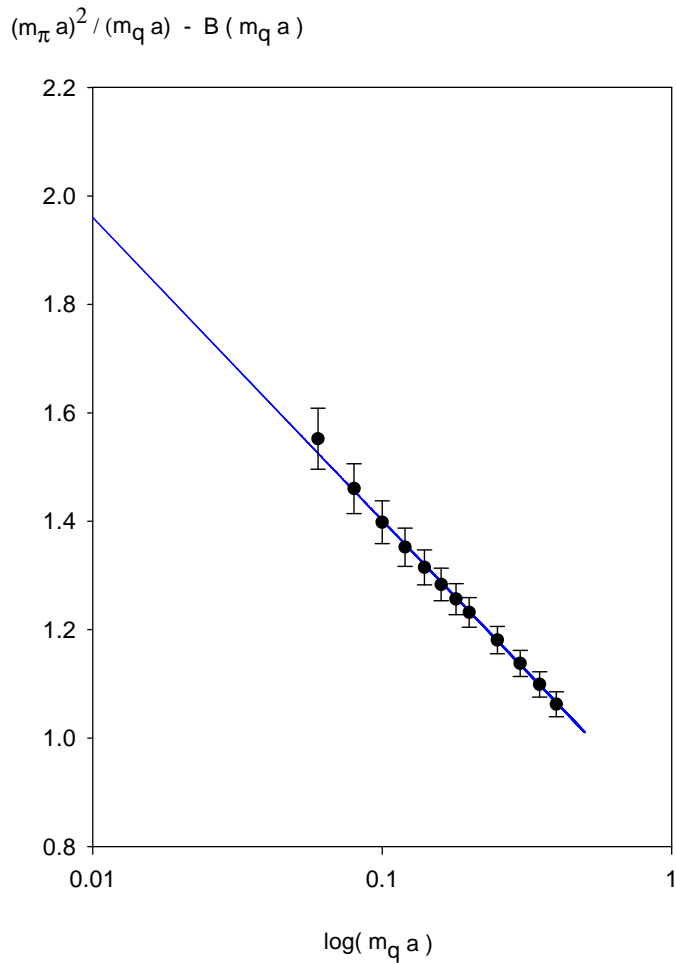


Figure 4: The extraction of quenched chiral logarithm by plotting  $(m_\pi a)^2 / (m_q a) - B(m_q a)$  versus  $\log(m_q a)$ . From the slope of the fitted straight line, the coefficient of quenched chiral logarithm can also be determined to be  $\delta = 0.2034 \pm 0.0140$ .

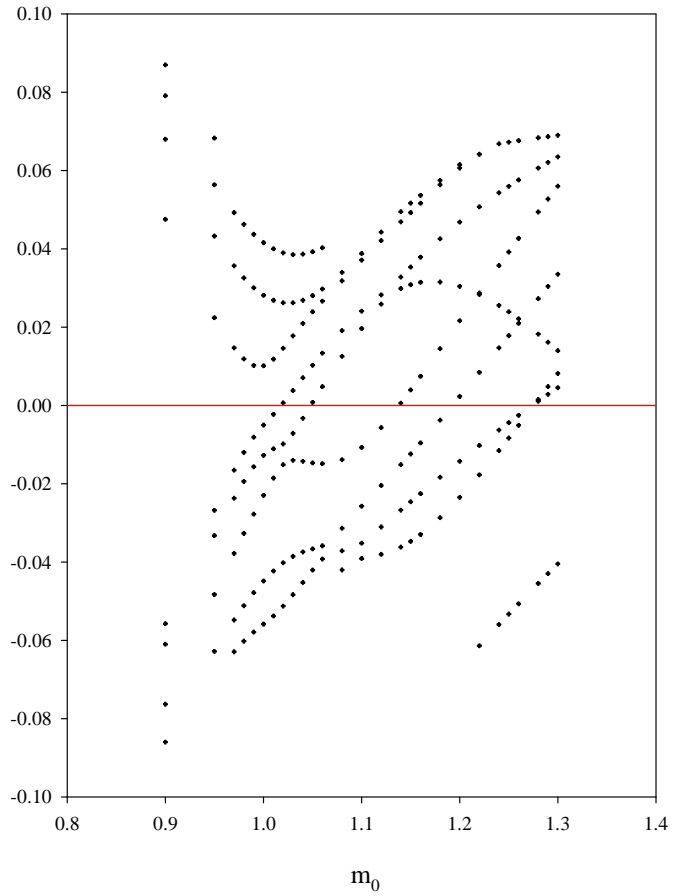


Figure 5: The spectral flow of 8 lowest-lying eigenvalues of  $H_w$  for the 50th gauge configuration. There are 6 crossings from negative to positive, so the index is equal to -6.

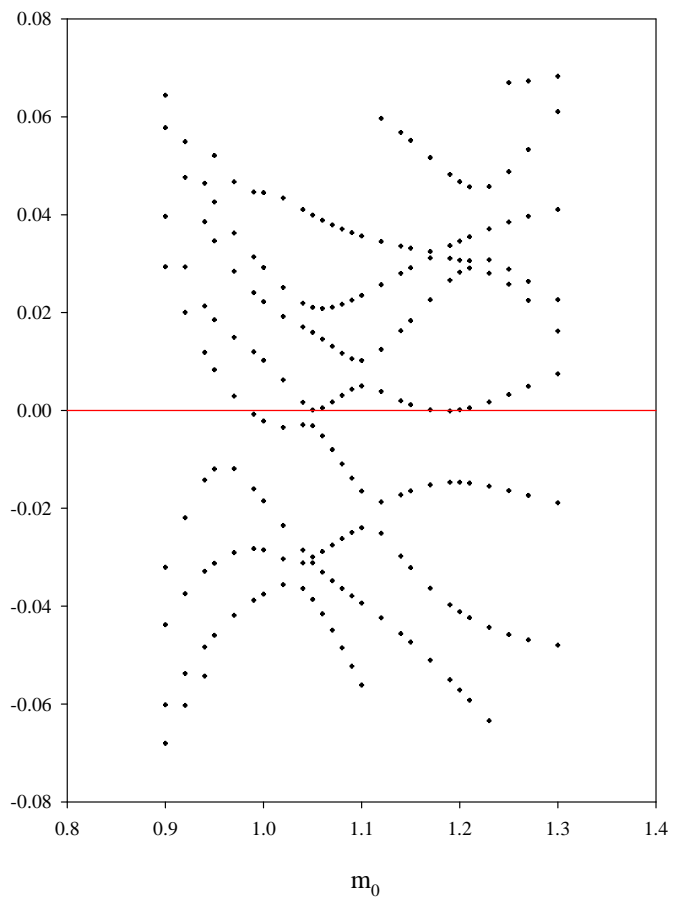


Figure 6: The spectral flow of 8 lowest-lying eigenvalues of  $H_w$  for the 8th gauge configuration. There is only one crossing from positive to negative around  $m_0 = 0.98$ , so the index is equal to  $+1$ .